Acta Crystallographica Section A
Foundations of Crystallography
ISSN 0108-7673

Received 12 February 2004
Accepted 13 July 2004

Electron-density studies of molecular magnetic materials

Sébastien Pillet, Mohamed Souhassou and Claude Lecomte*

Laboratoire de Cristallographie et Modélisation des Matériaux Minéraux et Biologiques, Université Henri Poincaré, UMR CNRS 7036, BP239, 54506 Vandoeuvre les Nancy, France. Correspondence e-mail: claude.lecomte@lcm3b.uhp-nancy.fr

For more than forty years, the experimental determination and analysis of electron densities have played a fundamental role in advances in the chemical bond concept. The present paper illustrates the application of this approach to the field of molecular magnetism with examples that recently appeared in the literature. Particular attention is attached to several classes of materials, purely organic free radicals, coordination compounds and organometallic complexes, which exhibit specific magnetic behaviors. It is shown to what extent the electron-density analysis can shed light on bonding aspects that are closely related to magnetic couplings. Relations between spin delocalization, spin polarization, superexchange and the characteristics of the electron density are described. The use of the topological theory of 'atoms in molecules' allows the possible magnetic interaction pathways to be located and defined, especially through weak intermolecular contacts. The complementarity with polarized neutron diffraction and spin-density modeling techniques is particularly evident from the chosen examples.

1. Introduction

Molecular-based magnetic materials have been the subject of intense investigations and developments over the past decades due to their potential applications in information storage devices (Kahn, 1993). Many new exciting physical properties have been recently discovered in this area like photo-induced magnetization, single-molecule quantum behavior or molecular bistability (Miller & Drillon, 2001, 2002, 2003, 2004). Such materials are based on assemblies of magnetic molecular entities, connected *via* covalent bonds, coordination interactions or weak intermolecular hydrogen bonds; their design takes therefore advantage of the specificities of molecular crystals. The resultant macroscopic magnetic properties rely on the nature and strength of the intra- and intermolecular interactions, whose interplay leads to isolated molecule behaviors (high-spin clusters), low-dimensional properties (bimetallic chains) or even three-dimensional magnetic ordering (ferromagnets). In this context, full understanding of the magnetic coupling mechanisms is required to conceive new materials with enhanced properties.

Several concepts and theoretical models of magnetic coupling have been developed and extended to molecular systems (Anderson, 1963; Hay *et al.*, 1975; Kahn & Briat, 1976*a*,*b*). These models are based on exchange interactions between two paramagnetic centers A and B (typically transition-metal ions), close enough that the corresponding atomic wavefunctions Φ_A and Φ_B overlap. For large A–B separation, like in $A-L-B$ ligand-bridged bimetallic systems, the interactions can be mediated by a diamagnetic open-shell moiety, acting not only as a spacer but also as a coupler; this is called superexchange. Anderson developed a theory of superexchange, relying on $A-L$ and $L-B$ σ covalent bonds, which has been extended to molecular systems by Kahn & Briat (1976*a*,*b*). In this latter formalism, Φ_A and Φ_B are treated as molecular orbitals partially delocalized (spin delocalization) and overlapping on the bridging ligand L, leading to magnetic exchange interactions. These spin carrying molecular units are interconnected in the solid state by usually weak interactions to give macroscopic magnetic properties. Detailed and rigorous descriptions of these models can be found in the literature (Kahn, 1993).

In the field of molecular magnetism, single-crystal polarized neutron diffraction affords great possibilities for the understanding of the mechanisms at the atomic level (Schweizer, 1997; Gillon, 1999; Ressouche, 1999). This technique allows reconstruction of the periodic spin-density distribution in the material using a multipolar model or a wavefunction approach; it has been applied to many organic free radicals and organometallic compounds. One of the great successes of spin-density analysis in molecular magnetism is that it has experimentally elucidated the role played by the spin delocalization and spin polarization effects (see below) in the superexchange interactions, especially in bimetallic complexes (Gillon, 1999).

It should be emphasized that superexchange, spin delocalization and spin polarization strongly rely on the covalency of the chemical bonds along the $A-L-B$ interaction pathway.

The electron-density (ED) analysis (Coppens, 1997) appears therefore as a fruitful approach to gain insights into the interaction mechanisms in molecular magnetic materials. Since the pioneering work of P. Coppens in 1967 (Coppens, 1967), it has become a powerful tool to investigate interatomic and intermolecular chemical bonds in solids. The ED is usually described using a pseudoatomic multipolar model where the atomic density is given by (Hansen & Coppens, 1978)

$$\rho(\mathbf{r}) = \rho_{\rm core}(r) + P_v\kappa^3\rho_{\rm val}(\kappa r) + \sum_{l=0}^{l_{\max}} \kappa'^3 R_l(\kappa' r) \sum_{m=0}^{+l} P_{lm\pm} y_{lm\pm}(\theta, \varphi), \quad (1)$$

where $\rho_{\rm core}(r)$ and $\rho_{\rm val}(r)$ are spherically averaged core and valence EDs calculated from high-accuracy wavefunctions for ground-state isolated atoms (typically Clementi Hartree–Fock; Clementi & Roetti, 1974). The ionic contribution to the chemical bond is parameterized by an atomic valence-shell population P_v and a contraction–expansion κ parameter taking into account electron-shielding effects. The deformation of the valence-electron shell is projected onto real spherical harmonics $y_{lm\pm}$.

Remarkable insights into the metal–ligand coordination interactions have been earned from ED studies, more particularly in terms of L to M σ donation and M to L π back bonding according to the Dewar–Chatt–Duncanson model (Dewar, 1951; Chatt & Duncanson, 1953). This explanation of coordination bonds has been widely applied to metal porphyrins for example (Lecomte *et al.*, 1986, 1999). In addition, the 3*d* ED of transition metals may be described either by multipolar expansion or as a product of atomic 3*d* orbitals, whose populations can therefore be obtained from the refined multipole parameters (Holladay *et al.*, 1983). In the Fe, Cr, Cu series of Tutton salts for instance (Figgis, Iversen *et al.*, 1993; Figgis *et al.*1998), good agreement was found between the 3*d* orbital populations derived from the experimental ED and those obtained from polarized neutron diffraction or crystal field theoretical calculations.

The 'atoms in molecules' theory, developed by R. F. Bader and co-workers (Bader, 1990), affords a great tool for the detailed quantitative analysis of the ED distribution. According to this approach, two atoms are bonded if they are connected by a line of maximum ED, called a bond path, on which lies a bond critical point [BCP, where $\nabla\rho(r_{\rm CP}) = \mathbf{0}$]. The corresponding interatomic bond is fully characterized by the topological properties of the ED at the BCP: $\rho(r_{\rm CP})$, $\nabla^2\rho(r_{\rm CP}) = \lambda_1 + \lambda_2 + \lambda_3$, where λ_{1-3} are the curvatures (eigenvalues of the Hessian) of the ED. The bond can be further classified as closed-shell interactions for low $\rho(r_{\rm CP})$ and $\nabla^2\rho(r_{\rm CP}) > 0$ and shared-shell interactions for high $\rho(r_{\rm CP})$ and $\nabla^2\rho(r_{\rm CP}) < 0$. The ellipticity of the bond, defined as $\varepsilon = 1 - |\lambda_1/\lambda_2|$, where λ_1 and λ_2 are the principal curvatures of the ED in the plane perpendicular to the bond ($\lambda_1 < \lambda_2 < 0$), is a measure of the departure from cylindrical symmetry of the ED at the BCP, and therefore indicates the departure from purely σ bond (π character). According to the topological formalism, the total charge density can be partitioned into atomic fragments whose delimiting surfaces (or interatomic surfaces) are defined by the zero-flux condition of the gradient field. The integration of the ED in the atomic basins yields topological atomic charges (Souhassou & Blessing, 1999).

The ED analysis has recently been used to obtain new insights into the interaction mechanisms of molecular magnetic compounds; in the following, we review chosen examples of such studies, most of them being performed in our laboratory. The first section deals with nitronyl nitroxide free radicals. In the second part, we focus our attention on a coordination compound, a hydroxo-bridged Cu^{II} complex. In the last part, we present results on organometallic systems for which the magnetic couplings are mediated by extended organic bridges. The reader is encouraged to read the original papers for more details.

2. Organic free radicals

The design of purely organic magnetic materials, and particularly of the α-nitronyl nitroxide family, whose general formula is given in scheme (I),

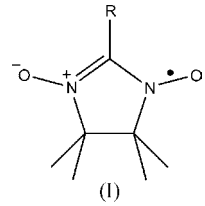

(I)

has attracted much attention since the discovery of the first genuine organic ferromagnet Nit(pNO$_2$)Ph (T_c = 0.6 K) (Osiecki & Ullman, 1968). Nitronyl nitroxide radicals consist of two nitroxide functions on which an unpaired electron is delocalized in a π^* molecular orbital [SOMO: singly occupied molecular orbital, (II)]

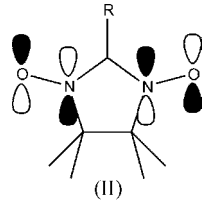

(II)

built from atomic N($2p_z$) and O($2p_z$) orbitals. Each radical behaves as a paramagnetic S = 1/2 unit whose interactions with neighboring radicals in the solid may lead to long-range magnetic ordering (bulk magnetism).

McConnell proposed two models to account for such long-range interactions by intermolecular contacts (McConnell, 1963, 1967). According to the first McConnell model, ferromagnetic interactions are attributed to intermolecular close contacts between atoms carrying spin populations of opposite sign; this follows from the simple application of Hund's rule in the intermolecular contact region. The second McConnell model, which has been developed to rationalize magnetic interactions in charge-transfer salts, relies on a mixing between the ground state and charge-transfer states corre-

sponding to an intermolecular spin transfer from the SOMO of one radical to the LUMO (lowest unoccupied molecular orbital) of a neighboring interacting radical. This process allows both antiferromagnetic and ferromagnetic interactions, the latter being predominant according to Hund's rule. An orbital description of this mechanism has been given by Kollmar & Kahn (1993). Several experimental spin-density analyses have revealed the transmission of magnetic interactions through hydrogen bonds, for example in the $[Co(NH_3)_5(H_2O)][Cr(CN)_6]$ coordination compound by Figgis, Kucharski & Vrtis (1993). However, no clear correlations between magnetic properties (nature and dimensionality) and geometrical characteristics of the intermolecular contacts have been found in nitronyl nitroxides, indicating that further investigations are still needed (Deumal *et al.*, 1999). To fully understand these mechanisms, several ED studies of free radicals have recently been undertaken (Yasui *et al.*, 2000; Pillet *et al.*, 2001; Claiser *et al.*, 2002; Ziessel *et al.*, 2004). We will discuss in the following results obtained on three nitronyl nitroxide radicals, namely 4,5-dihydro-4,4,5,5,-tetramethyl-2-[*p*-(methylthio)phenyl]imidazol-1-oxyl 3-oxide, 2-(6-ethynyl-2-pyridyl)-4,5-dihydro-4,4,5,5-tetramethylimidazol-1-oxyl 3-oxide and an ethylene-bridged bis(imidazol-1-oxyl 3-oxide), abbreviated as Nit(SMe)Ph (III), NitPy (IV) and D-NIT2 (V), respectively.

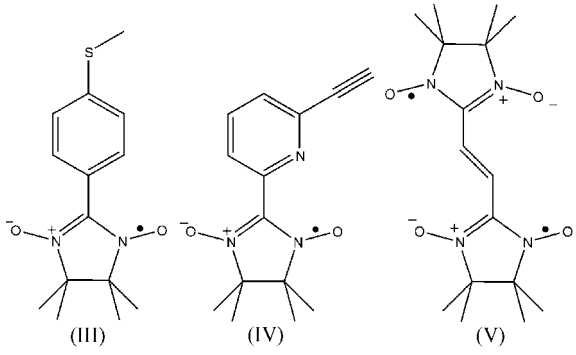

(III) (IV) (V)

The first one is a ferromagnet under T_c = 0.3 K (Caneschi, Ferraro, Gatteschi, Le Lirzin, Novak *et al.*, 1995; Caneschi, Ferraro, Gatteschi, Le Lirzin & Rentschler, 1995), NitPy exhibits ferromagnetic interactions and an antiferromagnetic ordering at T_N = 0.54 K (Romero *et al.*, 1996), whereas D-NIT2 is characterized by intramolecular antiferromagnetic couplings only (Ziessel *et al.*, 2004).

2.1. Electron-density specificities of the nitroxide N—O bond

The nitroxide group is a special case of chemical bond, with ED characteristics that differ notably from typical nitrate (Pillet, Souhassou, Lecomte *et al.*, 2004) and nitro bonds (Volkov, Abramov *et al.*, 2000; Volkov, Gatti *et al.*, 2000; Zhurova & Pinkerton, 2001; Kožíšek *et al.*, 2002; Kubicki *et al.*, 2002). From a structural point of view, the mean N—O distances parallel the corresponding bond orders: 1.277 (1) Å for nitroxide [mean over Nit(SMe)Ph, NitPy and D-NIT2], 1.239 (20) Å for nitrate and 1.218 (13) Å for nitro, with bond orders of 1.25, 1.3 and 1.5, respectively. Fig. 1 compares the corresponding static deformation densities. The three N—O groups exhibit similar features: two maxima of deformation density close to O atoms, attributed to lone pairs, and a high polarization of the bond deformation density clearly with a lower build-up in the nitroxide case. The position of the two O-atom lone pairs, directed at nearly 100° from the N—O axis, results from a high p_y character of the O-atom hybrid orbitals (x along N—O, z perpendicular to the map planes in Fig. 1), in contrast to the almost 120° angle and O-atom sp^2 formal hybridization in carbonyl groups (Coppens & Lehmann, 1976).

From the topological point of view, the nitroxide bond presents unusual and interesting properties. The N—O BCP is systematically displaced towards the N atom for nitro and nitrate, but almost centered in the bond for nitroxide with the corresponding ED in line with the bond-order and bond-length evolution: $2.63 < \rho_{\rm nitroxide} < 2.78$ e Å^{-3}, $2.87 < \rho_{\rm nitrate} < 3.10$ e Å^{-3} and $3.14 < \rho_{\rm nitro} < 3.47$ e Å^{-3}. Contrary to nitrate and nitro bonds, the Laplacian of the ED at the nitroxide BCP

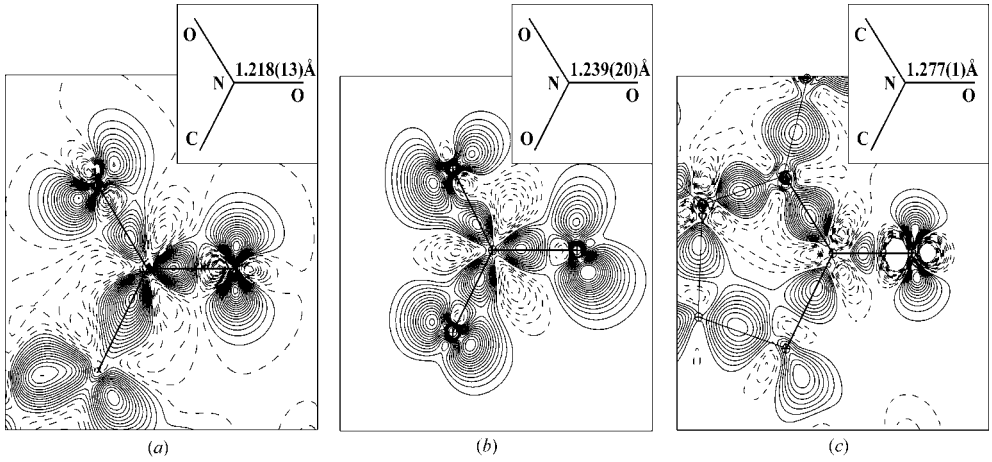

Figure 1
Static deformation density [ρ(calc multipolar) – ρ(calc spherical)] for (*a*) nitro in 1-phenyl-4-nitroimidazole (Kubicki *et al.*, 2002), (*b*) nitrate in $Cu_2(OH)_3(NO_3)$ (Pillet, Souhassou, Lecomte *et al.*, 2004) and (*c*) nitroxide in D-NIT2 (Ziessel *et al.*, 2004) groups. Contour levels ±0.05 e Å^{-3}, positive contours as solid lines and negative contours dashed. (*a*) and (*c*) reproduced with permission of the authors.

is rather small (from −3.4 to +2.78 e Å^{-5}) and even positive for Nit(SMe)Ph and NitPy. The positive sign of the Laplacian cannot be attributed to real closed-shell interactions but rather indicates ED depletion in the bonding region and correlated electron redistribution towards N and O atoms, which is in line with the presence of a single unpaired electron in the antibonding π^* orbital. Indeed, nitroxide bonds are characterized by a high λ_3 curvature along the bond path and low λ_1 and λ_2 curvatures in the perpendicular directions. The different behavior of the three N—O bond types is also evident from the inspection of the topological atomic charges. The nitro and nitrate N atoms are positive whereas the O atoms carry a highly negative charge, reflecting a polarization of the N—O bond. Contrary to this, the charge of the nitroxide group is shared between N and O atoms [q(N) < 0, q(O) < 0], consistent with a charge separation and electron redistribution from the bonding region towards N and O atoms. Experimental spin densities of nitronyl nitroxide radicals clearly demonstrate the π shape of the SOMO, built from N($2p_z$) and O($2p_z$) atomic orbitals with spin populations shared between N and O atoms (Pontillon *et al.*, 1999; Romero *et al.*, 2000). In summary, the ED distribution and its topological features, together with spin-density observations, clearly demonstrate the π^* antibonding nature of the SOMO.

2.2. Importance of conjugation and aromaticity in the interaction mechanisms

Besides the specific behavior of the two nitroxide groups, spin polarization, which is characterized by spin populations of alternating sign on the organic backbone neighboring the nitroxide functions, plays a major role in the magnetic coupling of nitronyl nitroxide free radicals. Spin polarization results from the mixing between the SOMO, HOMO (highest occupied molecular orbital) and LUMO frontier orbitals. It is conveniently described in terms of configuration interaction and mixing between the ground state and simply excited states As discussed above, the SOMO corresponds to an antibonding π^* orbital delocalized on the two nitroxide groups. For typical nitronyl nitroxides, the HOMO and LUMO are mainly delocalized on the substitution *R* fragment (I). Accordingly, it is expected that a highly conjugated *R* group might yield efficient spin polarization by mixing between the symmetry-adapted SOMO, LUMO and HOMO.

The topological properties of the ED in Nit(SMe)Ph show high conjugation effects from the nitroxide groups to the thiomethyl moiety (III) with ED, Laplacians and ellipticities at the BCPs along the conjugation path higher than for single bonds, which correlates well with spin polarization evidenced by polarized neutron diffraction. This conjugated backbone corresponds also exactly to the location of the LUMO as derived by Pontillon *et al.* (1999) from theoretical DFT calculations [depicted in (VI)].

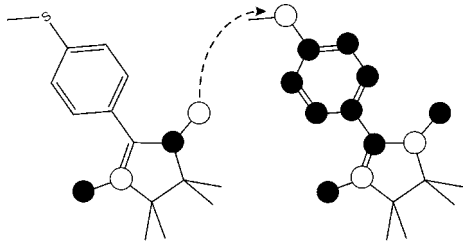

(VI)

The situation is more complex in NitPy for which the *R* fragment is a pyridine ring substituted by an ethynyl function (IV). As for Nit(SMe)Ph, high conjugation occurs from the ethynyl to the N—O groups, assisted by the pyridine N atom. This latter exerts a polarization of the pyridine ED, the C—N bonds withdrawing ED from the other pyridine C—C bonds. For NitPy, experimental spin densities show spin polarization on the pyridine ring and the ethynyl function (Romero *et al.*, 2000), in agreement with the ED derived conjugation scheme. In the bis-radical D-NIT2 (V), the bridging ethylene function presents also a high π character and therefore electron conjugation spread between the two nitronyl rings, in line with a dihedral angle of less than 2°. Correlatively, high spin polarization with alternating spin signs on the four bridging C atoms might be expected and has been discussed by Ziessel *et al.* (2004) from solid-state NMR spectroscopy.

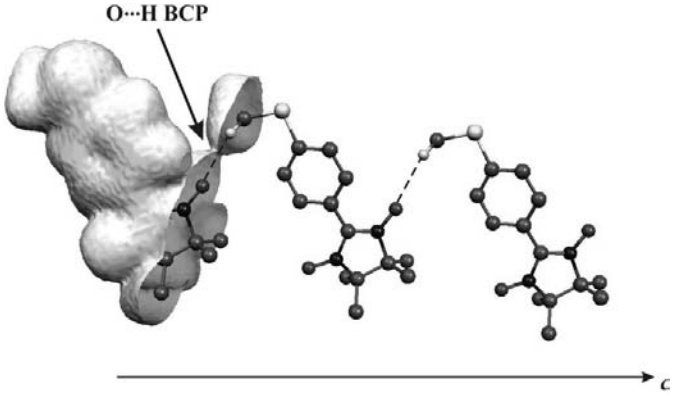

Figure 2
Intermolecular contacts along the *c* crystallographic axis of Nit(SMe)Ph (Pillet *et al.*, 2001). The total electron density is plotted at the 0.03 e Å^{-3} level. The H···O BCP [$d_{O\cdots H}$ = 2.506 (4) Å, $\rho(r_{CP})$ = 0.03 e Å^{-3}] is indicated by the arrow.

2.3. Interradical contacts and interaction pathways

Nitronyl nitroxide radicals exhibit macroscopic magnetic properties, resulting from long-range interaction in the solid. The ED distribution has been used in all three discussed examples to define possible interradical interaction pathways. In the atoms-in-molecules framework (Bader, 1990), the presence of a bond path, with a corresponding BCP and an interatomic surface are definite clues for the existence of a chemical bond. Fig. 2 presents the total ED of Nit(SMe)Ph along the crystallographic *c* axis, where a weak C—H···O hydrogen bond connects one nitroxide function to the thiomethyl group of a symmetry-related radical (cell translation along *c*). The observed bridge of ED is clear evidence that the radicals are not isolated in the crystal. This contact is further characterized by a bond path and a BCP with rather low ED

[$\rho(r_{CP}) = 0.03$ e Å^{-3}]. Similar weak hydrogen bonds have been pointed out by topological analysis in the other crystal directions. In NitPy, several interradical C—H···O and C—H···N hydrogen bonds, involving both nitroxide functions, have been located by Claiser *et al.* (2002), with ED at the BCPs higher than for Nit(SMe)Ph. In contrast, no significant interradical hydrogen bonds have been observed in D-NIT2, which accordingly behaves as an isolated biradical in the solid state.

2.4. Electron-density distribution and interaction mechanisms

From the joint analysis of spin and electron densities, one can postulate interaction mechanisms. In Nit(SMe)Ph, the experimental spin density evidences the localization of the unpaired electron in the π^* SOMO as well as spin-polarization effects on the phenyl ring and the bridging C atom. The topological analysis of the ED indicates a conjugated scheme from N—O to the S atom, which corresponds also to the localization of the LUMO. The methyl C atom of the thiomethyl group carries a significant spin population and a negative charge ($q_{CH_3} = -0.2$ e), opposite to the other methyl groups of the radical ($\langle q_{CH_3} \rangle = +0.3$ e). This methyl group is also involved in an interradical C—H···O hydrogen bond. The magnetic properties of Nit(SMe)Ph can therefore be explained according to the second McConnell mechanism by a SOMO to LUMO spin and electron transfer through a hydrogen bond, (VI).

The same conclusions on localization of the unpaired electron in the SOMO and spin polarization over the ethynyl-bridged pyridine ring are valid for NitPy. A conjugation scheme, corresponding to the location of the LUMO, is spread over the pyridine ring and the ethynyl function. An intermolecular C—H···O hydrogen bond between a nitroxide group and the ethynyl function, together with the spin population observed on the involved ethynyl H atom, indicate a SOMO to LUMO spin and electron transfer as for Nit(SMe)Ph. As concluded by Romero *et al.* (2000) and by Claiser *et al.* (2002), NitPy fulfils the conditions for an intermolecular magnetic coupling according to the second McConnell mechanism (VII), which might explain the observed ferromagnetic interactions.

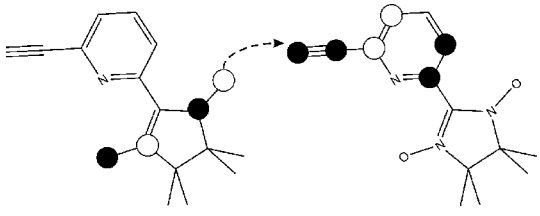

(VII)

At 0.54 K, NitPy undergoes an antiferromagnetic transition that could result from additional C—H···O and C—H···N interradical contacts in the solid (Claiser *et al.*, 2002).

Compared to the two previous examples, the behavior of D-NIT2 appears rather simple. An efficient intraradical π delocalization scheme through the bridging C═C double bond connects the two radicals, responsible for the antiferromagnetic coupling. No strong intermolecular contacts have been located that could overcome this coupling, leading to purely molecular magnetic properties, without long-range interactions.

3. Coordination complexes

The understanding of the superexchange interactions taking place between transition-metal ions coupled by a diamagnetic unit has raised considerable interest from a fundamental point of view. According to the models developed for oxides (Anderson, 1963; Goodenough, 1963) and extended to molecular complexes (Kahn & Briat, 1976*a*,*b*), the covalent bonds between the coupled transition metals and the diamagnetic bridging group play a fundamental role. Simple hydroxo-bridged copper(II) dimers have been the subject of particular attention, a simple empirical linear relation between the J exchange parameter and the Cu—O—Cu bridge angle has been derived by Crawford *et al.* (1976). Several experimental ED studies have been devoted to coordination compounds exhibiting indirect exchange interactions, among other Cu^{II} complexes: copper hydroxonitrate $Cu_2(OH)_3(NO_3)$ (Pillet, Souhassou, Lecomte *et al.*, 2004), azurite $Cu_3(CO_3)_2(OH)_2$ (Belokoneva *et al.*, 2001), dioptase $Cu_6(Si_6O_{18})\cdot 6H_2O$ (Belokoneva *et al.*, 2002) and transition-metal monoxides: MnO and CoO (Jauch & Reehuis, 2002, 2003).

3.1. $[Cu_2(OH)_3(NO_3)]$, an example of a hydroxo-bridged copper(II) complex

$[Cu_2(OH)_3(NO_3)]$ is a typical layer copper hydroxide whose crystal structure can be described as a two-dimensional triangular array of Cu atoms in two different Jahn–Teller distorted octahedral environments (Fig. 3) (Effenberger, 1983). Cu1 is surrounded by four hydroxo groups in the basal plane [$\langle Cu1—O_{basal} \rangle = 1.9650$ (8) Å] and two nitrate ions in the axial directions [$\langle Cu1—O_{axial} \rangle = 2.3959$ (8) Å], whereas Cu2 is coordinated by five hydroxo and one nitrate ion [$\langle Cu2—O_{basal} \rangle = 1.9948$ (7), $\langle Cu2—O_{axial} \rangle = 2.3454$ (7) Å]. According to the specific layer structure, $[Cu_2(OH)_3NO_3]$ is the archetype of Heisenberg antiferromagnetic ($S = 1/2$) interactions on a triangular lattice with weak interlayer couplings (Drillon *et al.*, 1995; Laget *et al.*, 1998; Massobrio *et al.*, 1999, 2001). This in-plane triangular geometry certainly leads to magnetic frustration effects. Among the planes, four different Cu···Cu exchange pathways (J1–4 in Fig. 3) can be isolated with intermetal distances from 3.03661 (5) to 3.2323 (2) Å; two of them involve two hydroxo ions whereas the other two rely on one hydroxo and one nitrate ion.

To explain the magnetic couplings in $[Cu_2(OH)_3(NO_3)]$, two mechanisms could be invoked: by direct overlap of the Cu1 and Cu2 d orbitals (direct exchange) or by superexchange through the bridging O atoms. The ED distribution and its topological analysis in the Cu···Cu interaction pathways bring some information on the Cu—O chemical bonding that can

help our understanding of the magnetic interactions. The Cu1 and Cu2 deformation densities reflect the populations of the atomic 3*d* orbitals due to the assumed D_{4h} crystal field (although the real symmetry is lower). Under D_{4h} point symmetry, the *d* orbitals split into four levels according to $a_{1g}(d_{z^2})$, $b_{1g}(d_{x^2-y^2})$, $b_{2g}(d_{xy})$ and $e_g(d_{xz},d_{yz})$, which agrees with the populations derived from the modeled ED (Table 1). The d_{xy}, d_{xz}, d_{yz} and d_{z^2} orbitals are fully occupied whereas $d_{x^2-y^2}$ is only partly filled; Cu1($d_{x^2-y^2}$) and Cu2($d_{x^2-y^2}$) are therefore the Cu magnetic orbitals. A similar observation has been made by Massobrio *et al.* (1999, 2001) from DFT calculations. If superexchange interactions occur, significant Cu—O σ overlap should be effective; hence the characterization of the Cu—O bond is fundamental. The ionic contribution to the Cu—O chemical bond is estimated from the topological charges which show a topological electron transfer from both Cu (q_{Cu1} = +1.0, q_{Cu2} = +0.94 e) to the hydroxo (q_{OH} = −0.39 e) and nitrate ions (q_{NO_3} = −0.76 e). On the other hand, the ED of the O and Cu atoms clearly overlap in the Cu—O region indicating a significant covalent character (Fig. 4), the overlap being more pronounced in the basal Cu—OH directions than in the axial Cu—OH and Cu—ONO_2 ones. The mean EDs at the corresponding BCPs are $\langle\rho_{Cu-O_{basal}}\rangle$ = 0.58 and $\langle\rho_{Cu-O_{axial}}\rangle$ = 0.24 e Å^{-3} with associated Laplacians of $\langle\nabla^2\rho_{Cu-O_{basal}}\rangle$ = 8.7 and $\langle\nabla^2\rho_{Cu-O_{axial}}\rangle$ = 3.1 e Å^{-5}.

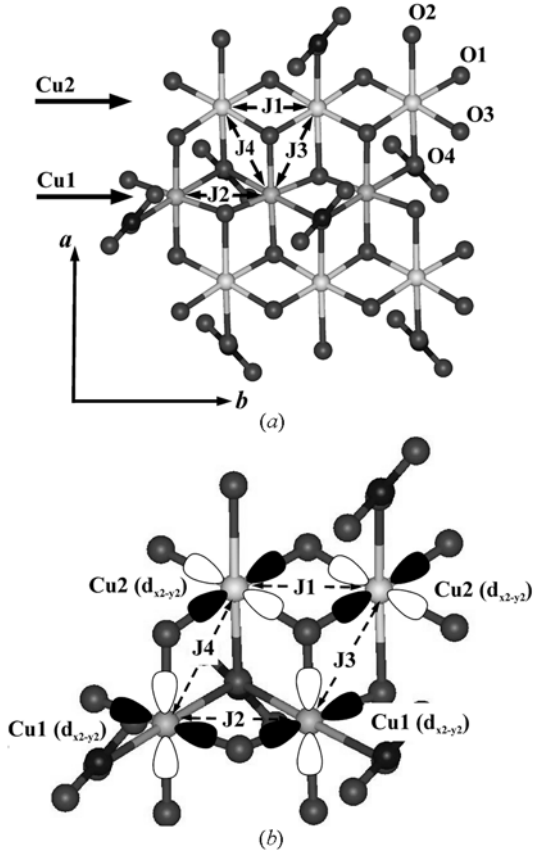

Figure 3
(*a*) Two-dimensional copper triangular lattice of the $[Cu_2(OH)_3NO_3]$ structure. *J*1,4 are the coupling constants corresponding to the four different Cu···Cu exchange pathways. (*b*) Orientation of the Cu $d_{x^2-y^2}$ atomic orbitals corresponding to *J*1,4 (Pillet, Souhassou, Lecomte *et al.*, 2004).

Table 1
Populations of the Cu 3*d* atomic orbitals in $Cu_2(OH)_3(NO_3)$ (in %).

	$d_{x^2-y^2}$	d_{z^2}	d_{xy}	d_{xz}	d_{yz}
Cu1	16.8 (6)	19.8 (5)	21.0 (5)	20.9 (5)	21.5 (6)
Cu2	14.4 (5)	21.3 (5)	19.8 (5)	21.0 (5)	23.5 (6)

The ED topology of the four Cu···Cu pathways consists of BCPs located in all the Cu—O bonds; no BCP lies directly in the Cu···Cu direction. Accordingly, the ED distribution does not show any evidence for a direct chemical bond between Cu atoms, but rather indirect interaction through the O atoms. The Cu1($d_{x^2-y^2}$) and Cu2($d_{x^2-y^2}$) magnetic orbitals are furthermore well oriented for efficient Cu—O σ overlaps (Fig. 3*b*). All these observations, significant covalency of the Cu—O bonds, occupancy of the 3*d* orbitals, orientation of the $d_{x^2-y^2}$ orbitals and absence of direct Cu···Cu bonding interactions are consistent with a superexchange mechanism mediated by the basal O atoms. The ED distribution does not however allow discussion of the sign and amplitude of the corresponding exchange interactions.

Weak interlayer exchange couplings have been observed from magnetic measurements that are correlated to three O···H hydrogen bonds between the nitrate and hydroxo ions. In these regions, bridges of ED connect the layers with ED at the BCPs corresponding to medium-strong hydrogen bonds that could possibly mediate the magnetic interactions.

4. Organometallic compounds

There has been considerable interest in the magnetic properties of *A*—*L*—*B* polymetallic complexes in which the *A* and *B* paramagnetic transition metals are connected by an extended *L* diamagnetic bridge like pyrimidine, oxalato, oxamato. In this class of compounds, the magnetic properties are due in most cases to superexchange interactions assisted by the organic bridge. In that context, low-dimensional

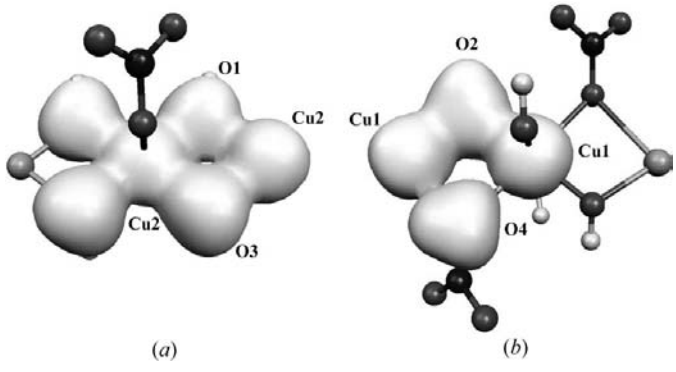

Figure 4
Total electron density in (*a*) the Cu2···Cu2 (*J*1 in Fig. 3) and (*b*) Cu1···Cu1 (*J*2 in Fig. 3) exchange pathways. The electron density is only plotted for a fragment of the structure with a 0.5 e Å^{-3} isocontour (Pillet, Souhassou, Lecomte *et al.*, 2004).

compounds with chain or layer topology represent model systems. In particular, infinite bimetallic Mn^{II}–Cu^{II} chains have been the subject of numerous studies, the high magnetic moment per (Mn^{II}—ligand—Cu^{II}) unit allowing intense coupling, despite the large Mn–Cu separation along the chains. Understanding the exact nature of the chemical bonding in the $A-L-B$ unit appears fundamental to better explain the superexchange mechanism in such materials. Several ED studies have been undertaken on polymetallic complexes, with the aim of describing in detail the chemical bonding of the pertinent magnetic units. Yasui *et al.* (2002) analyzed the behavior of pyrimidine-bridged copper $[Cu(NO_3)_2(H_2O)_2(pm)_2]$, iron and cobalt complexes $[MCl_2(pm)_2]$ (M = Co, Fe). Pillet, Souhassou, Mathonière & Lecomte (2004) studied an oxamato bridged Mn–Cu ferrimagnetic chain.

4.1. $[Cu(NO_3)_2(H_2O)_2(pm)_2]$, a pyrimidine-bridged copper chain complex

The crystal structure of $[Cu(NO_3)_2(H_2O)_2(pm)_2]$ (Fig. 5) consists of Cu^{II} ions in an octahedral CuN_2O_4 environment of two pyrimidine groups and two water molecules in the basal plane [d_{Cu-N} = 2.031 (2), $d_{Cu-O_{basal}}$ = 2.011 (2) Å] and two nitrate ions in the axial directions [$d_{Cu-O_{axial}}$ = 2.340 (2) Å]. The Cu octahedra are furthermore bridged by the pyrimidine groups to make infinite parallel chains [Cu···Cu = 5.737 (5) Å]. $[Cu(NO_3)_2(H_2O)_2(pm)_2]$ presents antiferromagnetic couplings (J = $-25\ cm^{-1}$) that have been attributed to superexchange mediated by the pyrimidine along the chains without interchain magnetic interactions (Yasui *et al.*, 2001). From extended Hückel calculations, Mohri *et al.* (1999) proposed an interaction model based on overlap between the Cu($d_{x^2-y^2}$) orbital and the pyrimidine molecular orbitals. Yasui *et al.* (2002) analyzed in detail the corresponding ED distribution, using high-resolution X-ray diffraction and multipolar modeling, to corroborate this mechanism. The Cu electron deformation density (Fig. 6) indicates a preferential occupancy of the d_{xy}, d_{xz}, d_{yz} and d_{z^2} atomic orbitals and a lower occupancy of the $d_{x^2-y^2}$ due to the D_{4h} crystal field exerted by the coordinating ligands. From the multipole parameters, the authors derived 3d orbital populations of 1.8 to 1.9 e for the d_{xy}, d_{xz}, d_{yz} and d_{z^2} orbitals and 1.28 e for the $d_{x^2-y^2}$. According to these populations, $d_{x^2-y^2}$ is the Cu atomic magnetic orbital. The model deformation density exhibits also high peaks close to N and O atoms, which correspond to the lone pairs directed towards the Cu atom and result in efficient σ overlap with the symmetry-adapted $d_{x^2-y^2}$ magnetic orbital, in agreement with the model of Mohri *et al.* (1999). A topological analysis of the ED distribution could further characterize the bonding interactions and magnetic mechanism in $[Cu(NO_3)_2(H_2O)_2(pm)_2]$.

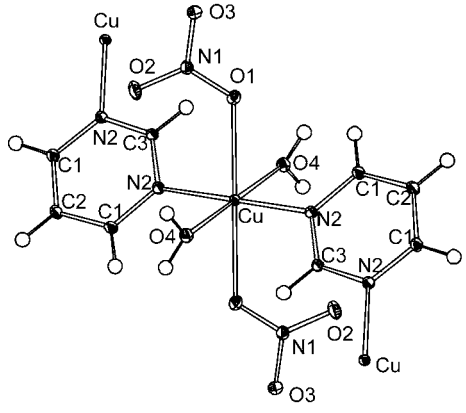

Figure 5
Molecular structure of $[Cu(NO_3)_2(H_2O)_2(pm)_2]$. Reproduced with permission from Yasui *et al.* (2002). Copyright (2002) Taylor and Francis.

4.2. $[MnCu(pba)(H_2O)_3]\cdot 2H_2O$, a ferrimagnetic chain compound

The crystal structure of $[MnCu(pba)(H_2O)_3]\cdot 2H_2O$, where pba stands for 1,3-propylenebis(oxamato) can be described as infinite parallel Mn—pba—Cu chains (Fig. 7) connected to each other by hydrogen bonds (Pei *et al.*, 1987). So $[MnCu(pba)(H_2O)_3]\cdot 2H_2O$ exhibits a magnetic behavior typical of ordered bimetallic chains, with one-dimensional

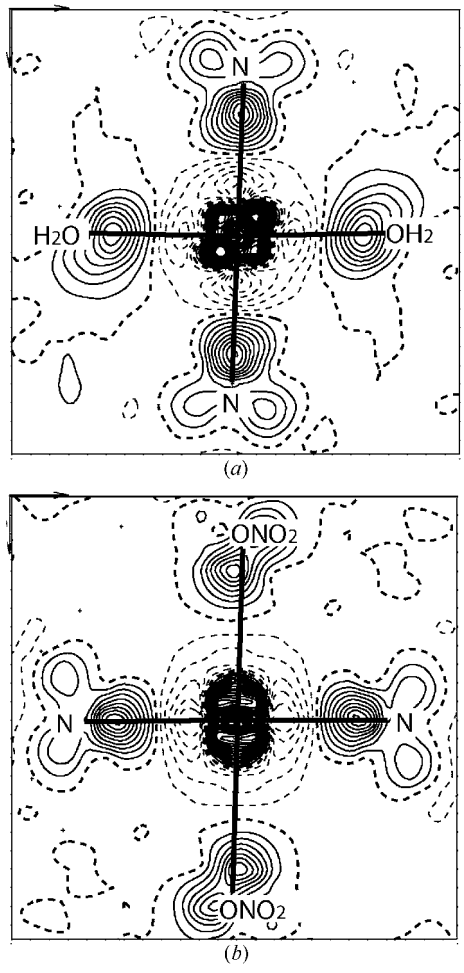

Figure 6
Model deformation density of $[Cu(NO_3)_2(H_2O)_2(pm)_2]$. Contours as in Fig. 1. Reproduced with permission from Yasui *et al.* (2002). Copyright (2002) Taylor and Francis.

antiferromagnetic interactions ($J = -23.4\ \mathrm{cm}^{-1}$) and weak interchain couplings. These properties have been investigated by polarized neutron diffraction measurements using a spin-density multipolar model by Baron *et al.* (1997), the negative and positive spin populations derived for Cu [$-0.75\ (2)\ \mu_B$] and Mn [$+4.93\ (3)\ \mu_B$] are characteristic of the antiferromagnetic interactions along the chains. In addition, spin densities have been observed on the oxamato moiety with positive contributions on the O atoms connected to Mn atoms and negative populations on all the other atoms. Baron *et al.* (1997) and Kahn *et al.* (1997) have thus explained the magnetic interactions between Mn and Cu by a spin delocalization mechanism through the oxamato bridge.

The ED distribution of $[MnCu(pba)(H_2O)_3]\cdot 2H_2O$ allows one to obtain further insights into the intrachain interactions. These are first characterized by high topological electron transfer from both metals ($q_{Cu} = +1.56$, $q_{Mn} = +1.45$ e) to the oxamato bridge ($q_{oxamato} = -1.54$ e) which undergoes in turn a charge polarization with positive inner C atoms ($\langle q_C \rangle = 1.12$ e) and negative coordinating N and O atoms ($q_N = -1.15$, $\langle q_O \rangle = -0.88$ e). In addition to the electron-transfer contribution, high overlap between the Cu 3*d* atomic orbitals and the molecular orbitals of the oxamato moiety is evidenced by high ED at the corresponding Cu—O [$\rho(r_{CP}) = 0.62$ e Å^{-3}] and Cu—N [$\rho(r_{CP}) = 0.74$ e Å^{-3}] BCPs. The covalency is even more pronounced for the Cu—N bond. By comparison to the promolecule (independent-atom model), an increase of ED of as much as +0.17 and 0.22 e Å^{-3} occurs in the Cu—O and Cu—N bonds, respectively. On the other hand, the topological properties of the Mn—O bonds correspond to closed-shell interaction with lower covalency [$\langle \rho(r_{CP}) \rangle = 0.37$, +0.10 e Å^{-3} with respect to the promolecule]. This difference of behavior is particularly evident from inspection of Fig. 8.

The Cu 3*d* orbital populations, derived from the multipole parameters of the Cu deformation density, are 24.6 (3)% for the d_{xy}, d_{yz}, d_{xz} orbitals and 11.1 (3) and 16.5 (3)% for the $d_{x^2-y^2}$ and d_{z^2} orbitals, respectively, in agreement with the CuN_2O_3 pyramidal environment. According to Hund's rule, the d_{z^2} orbital is likely to be partly filled by spin-up and spin-down electrons, whereas $d_{x^2-y^2}$ can accept one single-spin electron and represents therefore the Cu atomic magnetic orbital.

The topological properties of all BCPs of the oxamato bridge show characteristic features of conjugation effects: short bond lengths, high EDs, high Laplacians and high ellipticities; this electron conjugation is necessary to mediate the interactions along the chain according to the super-exchange mechanism proposed by Baron *et al.* (1997). Indeed, the Cu $d_{x^2-y^2}$ orbital is σ overlapping with the corresponding molecular orbital of the oxamato bridge. Since this latter presents high electron conjugation, spin can be transferred from the Cu atom to the oxamato group by spin delocalization (Baron *et al.*, 1997). According to the stronger Cu—N overlap, this phenomenon is expected to be more efficient through the N atom. A similar argument holds for the Mn atom but with a lower effect due to lower Mn—O overlap in agreement with the lower Mn-bridge spin delocalization discussed by Kahn *et al.* (1997).

The magnetic behavior of $[MnCu(pba)(H_2O)_3]\cdot 2H_2O$ presents a departure from one-dimensional antiferromagnetic exchange coupling at very low temperatures (below 2.3 K). As shown in Fig. 9, bridges of ED connect the chains by hydrogen bonds with ED values at the corresponding BCPs from 0.15 to

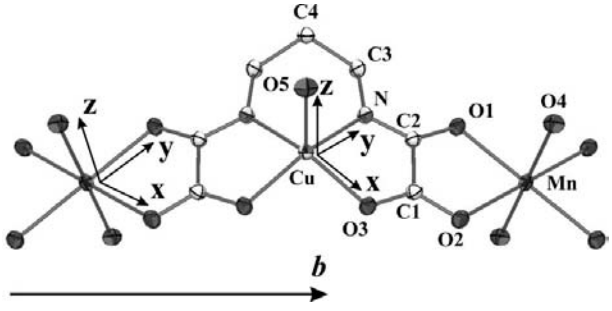

Figure 7
Chain structure of $[MnCu(pba)(H_2O)_3]\cdot 2H_2O$ and local coordinate systems for Mn and Cu atoms. Thermal displacement ellipsoids are plotted at the 50% probability level. H atoms and non-coordinated water molecules are omitted for clarity (Pillet, Souhassou, Mathonière & Lecomte, 2004).

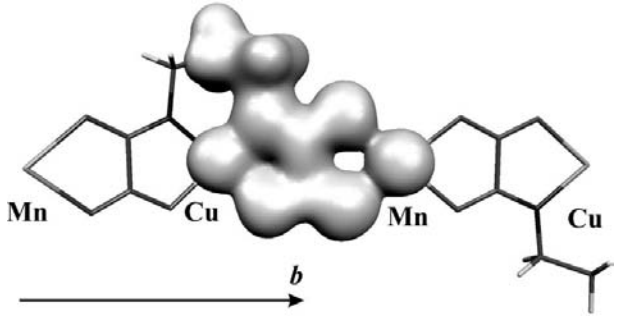

Figure 8
Total electron density along the chain of $[MnCu(pba)(H_2O)_3]\cdot 2H_2O$ with an isocontour of 0.25 e Å^{-3} (Pillet, Souhassou, Mathonière & Lecomte, 2004).

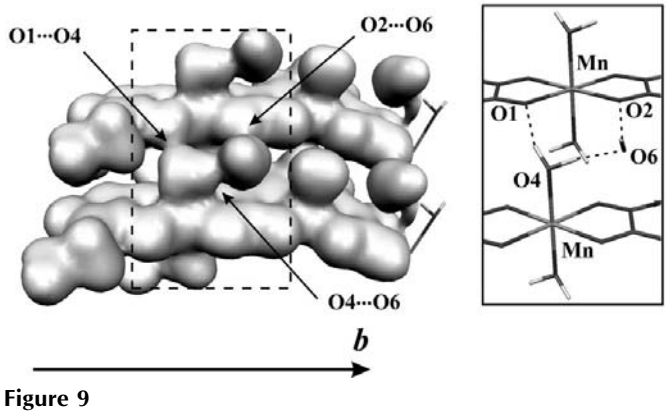

Figure 9
Total electron density in the interchain region of MnCu(pba)-$(H_2O)_3\cdot 2H_2O$ with an isocontour of 0.1 e Å^{-3}. The interchain hydrogen bonds (O1···O4, O2···O6 and O4···O6) are given in the insert (Pillet, Souhassou, Mathonière & Lecomte, 2004).

0.30 e Å^{-3} and indicate medium-strong hydrogen bonds. These contacts might be involved in the interchain magnetic couplings.

5. Conclusions

Even if polarized neutron diffraction is at present one of the most widely used and powerful techniques for investigating magnetic interaction mechanisms in molecular solids, analysis of the experimental electron-density distribution gives valuable insights into bonding aspects that can be related to magnetic couplings.

In transition-metal-containing systems, the electron deformation density at the metal site allows derivation of the 3*d* orbital populations whose anisotropy reflects the lift of degeneracy due to the crystal field. From the inspection of the 3*d* orbital populations, the atomic magnetic orbital can be defined; this is particularly evident in elongated octahedral copper(II) complexes where the Cu($d_{x^2-y^2}$) orbital carries the unpaired electron. In addition, the topology of the electron-density distribution allows discrimination between direct or indirect Metal···Metal bonding by the spatial distribution of bond paths and bond critical points. In the case of hydroxo-bridged copper(II) dimers for instance, the absence of a BCP in the Cu···Cu direction is direct evidence of indirect coupling mediated by the bridging hydroxo and nitrate ions.

The ED analysis is also very efficient in locating intermolecular contacts like hydrogen bonds. Indeed, the presence of a bond path on which lies a bond critical point in the intermolecular region indicates a bonding interaction, usually weak, that can mediate magnetic couplings in the solid. This approach has been used for locating possible interradical, interplane and interchain contacts in most of the compounds described above.

All the results discussed here are related to purely organic materials or first-row transition-metal complexes. Many rare-earth or second-row transition-metal complexes exhibit interesting magnetic properties and are nowadays more and more designed. The investigation of the electron-density distribution of molecular magnetic complexes containing such heavy elements is a real challenge that has already been attempted (Claiser *et al.*, 2004). The results obtained are encouraging but need very accurate diffraction experiments and, in the case of rare-earth complexes, very accurate scattering factors.

The authors are indebted to the Université Henri Poincaré, the French Minister of Research and Technology and the CNRS for financial support. We wish to thank all our colleagues involved in part of the work presented here, Y. Pontillon, A. Caneschi, D. Gatteschi, C. Mathonière, P. Rabu, C. Massobrio, Y. Pouillon, M. Drillon and N. Claiser for fruitful discussions and support. We are grateful to Professor Masanori Yasui for making his work available to us.

References

Anderson, P. W. (1963). *Solid State Phys.* **14**, 99–214.
Bader, R. F. W. (1990). *Atoms in Molecules. A Quantum Theory*. *International Series of Monographs on Chemistry*, No. 22. Oxford: Clarendon Press.
Baron, V., Gillon, B., Cousson, A., Mathonière, C., Kahn, O., Grand, A., Ohrstrom, L., Delley, B., Bonnet, M. & Boucherle, J. X. (1997). *J. Am. Chem. Soc.* **119**, 3500–3506.
Belokoneva, E. L., Gubina, Y. K. & Forsyth, J. B. (2001). *Phys. Chem. Miner*. **28**, 498–507.
Belokoneva, E. L., Gubina, Y. K., Forsyth, J. B. & Brown, P. J. (2002). *Phys. Chem. Miner*. **29**, 430–438.
Caneschi, A., Ferraro, F., Gatteschi, D., Le Lirzin, A., Novak, M., Rentschler, E. & Sessoli, R. (1995). *Adv. Mater.* **7**, 476–478.
Caneschi, A., Ferraro, F., Gatteschi, D., Le Lirzin, A. & Rentschler, E. (1995). *Inorg. Chim. Acta*, **235**, 159–164.
Chatt, J. & Duncanson, L. A. (1953). *J. Chem. Soc.* pp. 2939–2947.
Claiser, N., Gillon, B., Souhassou, M., Lecomte, C., Hansen, N. K., Pontillon, Y., Caneschi, A., Gatteschi, D., Carbonera, C., Bencini, A., Cousson, A. & Lelièvre-Berna, E. (2004). *J. Phys. Chem Solids.* In the press.
Claiser, N., Souhassou, M., Lecomte, C., Pontillon, Y., Romero, F. & Ziessel, R. (2002). *J. Phys. Chem. B*, **106**, 12896–12907.
Clementi, E. & Roetti, C. (1974). *At. Data Nucl. Data Tables*, **14**, 177–478.
Coppens, P. (1967). *Science*, **158**, 1577–1579.
Coppens, P. (1997). *X-ray Charge Densities and Chemical Bonding*. IUCr/Oxford University Press.
Coppens, P. & Lehmann, M. S. (1976). *Acta Cryst.* B**32**, 1777–1784.
Crawford, V. H., Richardson, H. W., Wasson, J. R., Hodgson, D. J. & Hattfield, W. E. (1976). *Inorg. Chem.* **15**, 2107–2110.
Deumal, M., Cirujeda, J., Veciana, J. & Novoa, J. J. (1999). *Chem. Eur. J.* **5**, 1631–1642.
Dewar, M. J. S. (1951). *Bull. Soc. Chim. Fr.* p. C71.
Drillon, M., Hornick, C., Laget, V., Rabu, P., Romero, F. M., Rouba, S., Ulrich, G. & Ziessel, R. (1995). *Mol. Cryst. Liq. Cryst.* **273**, 663–678.
Effenberger, H. (1983). *Z. Kristallogr.* **165**, 127–135.
Figgis, B. N., Iversen, B. B., Larsen, F. K. & Reynolds, P. A. (1993). *Acta Cryst.* B**49**, 794–806.
Figgis, B. N., Kucharski, E. S. & Vrtis, M. (1993). *Z. Naturforsch. Teil A*, **48**, 123–126.
Figgis, B. N., Sobolev, A. N., Young, D. M., Schultz, A. J. & Reynolds, P. A. (1998). *J. Am. Chem. Soc.* **120**, 8715–8723.
Gillon, B. (1999). *Mol. Cryst. Liq. Cryst.* **335**, 53–72.
Goodenough, J. B. (1963). *Magnetism and the Chemical Bond*. New York: Interscience Publishers.
Hansen, N. K. & Coppens, P. (1978). *Acta Cryst.* A**34**, 909–921.
Hay, P. J., Thibeault, J. C. & Hoffmann, R. (1975). *J. Am. Chem. Soc.* **97**, 4884–4899.
Holladay, A., Leung, P. & Coppens, P. (1983). *Acta Cryst.* A**39**, 377–387.
Jauch, W. & Reehuis, M. (2002). *Phys. Rev. B*, **65**, 125111.
Jauch, W. & Reehuis, M. (2003). *Phys. Rev. B*, **67**, 184420.
Kahn, O. (1993). *Molecular Magnetism*. New York: VCH.
Kahn, O. & Briat, B. (1976*a*). *J. Chem. Soc. Faraday Trans. 2*, **72**, 268–281.
Kahn, O. & Briat, B. (1976*b*). *J. Chem. Soc. Faraday Trans. 2*, **72**, 1441–1447.
Kahn, O., Mathonière, C., Srinivasan, B., Gillon, B., Baron, V., Grand, A., Ohrstrom, L. & Ramasesha, S. (1997). *New J. Chem.* **21**, 1037–1045.
Kollmar, C. & Kahn, O. (1993). *Acc. Chem. Res.* **26**, 259–265.
Kožíšek, J., Hansen, N. K. & Fuess, H. (2002). *Acta Cryst.* B**58**, 463–470.
Kubicki, M., Borowiak, T., Dutkiewicz, G., Souhassou, M., Jelsch, C. & Lecomte, C. (2002). *J. Phys. Chem.* **106**, 3706–3714.

Laget, V., Hornick, C., Rabu, P., Drillon, M., Turek, P. & Ziessel, R. (1998). *Adv. Mater.* **10**, 1024–1028.
Lecomte, C., Blessing, R. H., Coppens, P. & Tabard, A. (1986). *J. Am. Chem. Soc.* **108**, 6942–6950.
Lecomte, C., Rohmer, M. M. & Benard, M. (1999). *The Porphyrin Handbook*, Vol. 7, edited by K. M. Kadish, K. M. Smith & R. Guilard. New York: Academic Press.
McConnell, H. M. (1963). *J. Phys. Chem.* **39**, 1910.
McConnell, H. M. (1967). *Proc. R. A. Welch Found. Conf. Chem. Res.* **11**, 144.
Massobrio, C., Pouillon, Y., Rabu P. & Drillon, M. (2001). *Polyhedron*, **20**, 1305–1314.
Massobrio, C., Rabu, P., Drillon, M. & Rovira, C. (1999). *J. Phys. Chem. B*, **103**, 9387–9391.
Miller, J. & Drillon, M. (2001). *Magnetism: Molecules to Materials I.* New York: VCH.
Miller, J. & Drillon, M. (2002). *Magnetism: Molecules to Materials II.* New York: VCH.
Miller, J. & Drillon, M. (2003). *Magnetism: Molecules to Materials III.* New York: VCH.
Miller, J. & Drillon, M. (2004). *Magnetism: Molecules to Materials IV*. New York: VCH.
Mohri, F., Yoshizawa, K., Yamabe, T., Ishida, T. & Nogami, T. (1999). *Mol. Eng.* **8**, 353–373.
Osiecki, J. H. & Ullman, E. F. (1968). *J. Am. Chem. Soc.* **90**, 1078–1079.
Pei, Y., Verdaguer, M., Kahn, O., Sletten, J. & Renard, J. P. (1987). *Inorg. Chem.* **26**, 138–143.
Pillet, S., Souhassou, M., Lecomte, C., Rabu, P., Massobrio, C. & Drillon, M. (2004). In preparation.
Pillet, S., Souhassou, M., Mathonière, C. & Lecomte, C. (2004). *J. Am. Chem. Soc.* **126**, 1219–1228.
Pillet, S., Souhassou, M., Pontillon, Y., Caneschi, A., Gatteschi, D. & Lecomte, C. (2001). *New J. Chem.* **25**, 131–143.
Pontillon, Y., Caneschi, A., Gatteschi, D., Grand, A., Ressouche, E., Sessoli, R. & Schweizer, J. (1999). *Chem. Eur. J.* **5**, 3616–3624.
Ressouche, E. (1999). *Physica (Utrecht) B*, **267–268**, 27–36.
Romero, F. M., Ziessel, R., Bonnet, M., Pontillon, Y., Ressouche, E., Schweizer, J., Delley, B., Grand, A. & Paulsen C. (2000). *J. Am. Chem. Soc.* **122**, 1298–1309.
Romero, F. M., Ziessel, R., De Cian, A., Fischer, J. & Turek, P. (1996). *New J. Chem.* **20**, 919–924.
Schweizer, J. (1997). *Physica (Utrecht)*, B**234–236**, 772–779.
Souhassou, M. & Blessing, R. H. (1999). *J. Appl. Cryst.* **32**, 210–217.
Volkov, A., Abramov, Y., Coppens, P. & Gatti, C. (2000*b*). *Acta Cryst.* A**56**, 332–339.
Volkov, A., Gatti, C., Abramov, Y. & Coppens, P. (2000*a*). *Acta Cryst.* A**56**, 252–258.
Yasui, M., Ishikawa, Y., Akiyama, N., Ishida, T., Nogayami, T. & Iwasaki, F. (2001). *Acta Cryst.* B**57**, 288–295.
Yasui, M., Kan-nari, E., Ishida, T., Nogami, T. & Iwasaki, F. (2000). *Bull. Chem. Soc. Jpn*, **73**, 1333–1340.
Yasui, M., Takayama, R., Akiyama, N., Hashizume, D. & Iwasaki, F. (2002). *Mol. Cryst. Liq. Cryst.* **376**, 519–524.
Zhurova, E. & Pinkerton, A. A. (2001). *Acta Cryst.* B**57**, 359–365.
Ziessel, R., Stroh, C., Heise, H., Raudaschl-Sieber, G., Köhler, F. H., Turek, P., Claiser, N., Souhassou, M. & Lecomte, C. (2004). *J. Am. Chem. Soc*. In the press.